CONFIDENTIAL

Copy
RM L54L17

NACA RM L54L17

TECH LIBRARY KAFB, NM
0144541

NACA

RESEARCH MEMORANDUM

CHARACTERISTICS OF LOADS IN ROUGH AIR AT TRANSONIC SPEEDS OF ROCKET-POWERED MODELS OF A CANARD AND A CONVENTIONAL-TAIL CONFIGURATION

By A. James Vitale

Langley Aeronautical Laboratory
Langley Field, Va.

(Unclassified)

NASA Tech Pub Announcement #4

CHANGE)

By... 14 Mar 55

GRADE OF OFFICER MAKING CHANGE)

14 Mar 61

CLASSIFIED DOCUMENT

This material contains information affecting the National Defense of the United States within the meaning of the espionage laws, Title 18, U.S.C., Secs. 793 and 794, the transmission or revelation of which in any manner to an unauthorized person is prohibited by law.

NATIONAL ADVISORY COMMITTEE
FOR AERONAUTICS

WASHINGTON

March 1, 1955

CONFIDENTIAL

TECH LIBRARY KAFB, NM
0143541

.R

NACA RM L54L17

[redacted]

NATIONAL ADVISORY COMMITTEE FOR AERONAUTICS

RESEARCH MEMORANDUM

CHARACTERISTICS OF LOADS IN ROUGH AIR AT TRANSONIC SPEEDS OF ROCKET-POWERED MODELS OF A CANARD AND A CONVENTIONAL-TAIL CONFIGURATION

By A. James Vitale

SUMMARY

Results from flight tests at transonic speeds are presented for a canard and a conventional-tail (or tail-last) rocket-powered model in continuous rough air. The use of an airspeed-fluctuation instrument for measuring the turbulence intensity experienced by the models is described, along with the resulting improvement in the technique of testing rocket models in rough air. The limitations of the technique for measuring small-order effects are also discussed.

The short-period frequency was dominant in the center-of-gravity normal-acceleration response for both models. The variation of load intensity with Mach number for the canard and tail-last models is compared with results from a tailless model previously tested to show the effect of improving the damping in pitch. A comparison of the canard and tail-last models indicated that the load intensity was about the same order of magnitude for both models at Mach numbers from 0.80 to 1.0 and any small-order effects were masked in the large scatter of the test results.

INTRODUCTION

The need for additional experimental techniques for studying gust loads on airplanes and missiles at transonic and supersonic speeds has led to an investigation of the use of rocket-powered models for gust-loads studies. The results from the exploratory investigation are presented in reference 1 in the form of a testing technique and procedure, along with experimental data on a tailless swept-wing rocket-powered model for flight through continuous rough air. The data presented in reference 1 promulged two main conclusions: (1) The low damping in pitch of the tailless model gave rise to a sizable amplification of loads

[redacted] CONFIDENTIAL

[redacted]

in rough air and (2) the testing technique as described (in ref. 1) was feasible and practical, but the precision was such that only large-order effects could be investigated. In addition, several improvements for the technique and instrumentation were suggested in reference 1.

The purpose of the present investigation was to develop further the testing technique and obtain gust-loads data on two additional rocket-powered models both of which had improved damping in pitch over the tailless model as shown in reference 2. The two models had 45° sweptback wings of aspect ratio 6 and NACA 65A009 airfoil section which were identical to those of the tailless model of reference 1. Improved damping was obtained by the addition of tail surfaces. For one model a canard surface was added and for the other the tail was added in the conventional or tail-last position.

As in reference 1, the test procedure involved testing the models in clear-air atmospheric turbulence associated with post-cold-front conditions. A survey airplane was used in choosing the test days and in determining the variation of turbulence intensity with altitude. The present investigation differed from reference 1 in that the models were equipped with an independent system for measuring the turbulence in the horizontal direction.

In the evaluation of the test results and in the associated theoretical calculations presented, extensive use is made of the techniques of generalized harmonic analysis. The test results are presented in the form of time histories, power spectra, and root-mean-square normal-acceleration increments for Mach numbers from 0.80 to 1.0 for both the canard and tail-last models. In addition, comparisons are made of the variation of root-mean-square normal-acceleration increments with Mach number of the tail-last, canard, and tailless (ref. 1) models to illustrate the overall effect on gust loads of improving the damping in pitch of both the tail-last and canard models over the tailless model.

SYMBOLS

A	aspect ratio, b^2/S
b	total wing span, ft
c	chord, ft
$\bar{c}$	mean aerodynamic chord, ft
f	frequency, cps
g	acceleration due to gravity, 32.2 ft/sec^2

h	altitude, ft
I_Y	moment of inertia about transverse axis, slug-ft^2
l	distance between center-of-gravity and nose accelerometers, ft
M	Mach number
Δn	normal-acceleration increment, g units
S	total wing area, sq ft
t	time, sec
$T_{1/2}$	time to damp to one-half amplitude, sec
W	weight, lb
V	velocity, ft/sec
K	constant in equation of power spectrum of gust velocity, $\Phi_i(\Omega) = \frac{K}{\Omega^2}$
σ	root-mean-square Δn, g units
ω_n	undamped natural frequency, radians/sec
$\Phi()$	power-spectral-density function of an arbitrary disturbance with respect to f or Ω
$\Phi_o()$	power-spectral-density function of output or normal acceleration
$\Phi_i()$	power-spectral-density function of input or gust velocity
Ω	reduced frequency, $2\pi f/V$, radians/ft

MODELS AND INSTRUMENTATION

Models

A canard and a tail-last configuration having 45° sweptback wings of aspect ratio 6 and NACA 65A009 airfoil section parallel to the free stream

were used in the present investigation. The tail surfaces were swept back 45° and had an aspect ratio of 4 and NACA 65A006 airfoil sections. The principal features of the models are shown in figures 1 to 3. The fuselage for both models was similar to that of the tailless model of reference 1 with a cylindrical section added at the fuselage maximum diameter. The fuselage ordinates are given in reference 2. Flat-plate aluminum-alloy fins were used to stabilize the models directionally. Listed in table I are the important physical characteristics of the models.

Instrumentation

Both the canard and tail-last models were equipped with a four-channel telemeter transmitting measurements of normal acceleration from accelerometers at the center of gravity and in the nose of the model, total pressure, and fluctuations in total pressure. The natural frequency and damping ratio of the accelerometers are given in the following table:

Accelerometer	Canard model		Tail-last model	
	f_n, cps	Damping ratio	f_n, cps	Damping ratio
Center of gravity	78	0.69	84	0.52
Nose	81	.70	79	.70

Amplitude-response corrections for the accelerometers were not made for frequencies up to 35 cps. The nose accelerometers were located approximately 3 feet ahead of the center of gravity for both models. Ground instrumentation included a CW Doppler radar set for obtaining model velocity, a modified SCR 584 radar set for obtaining model position in space, and a radiosonde for obtaining atmospheric conditions.

The need for an instrument to measure the turbulence experienced by the models led to the development of a device for measuring horizontal-gust fluctuations or fluctuations in total pressure. The problem encountered for the rocket-powered models was the difficulty of accurately measuring fluctuations in total pressure (due to gusts) which were a very small percentage of the steady-state pressure. A differential pressure cell was adapted for this purpose and was installed in the models for development purposes. A schematic drawing of the instrument is shown in the following sketch:

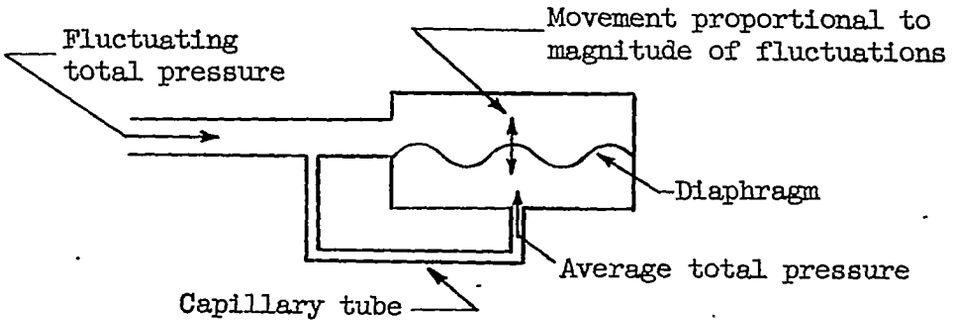

The differential cell is connected in such a way that one side of its diaphragm is exposed to the source of fluctuating total pressure and the other side of the diaphragm is connected to a source of reference pressure whose amplitude is equal to the average of the fluctuating total pressure. This average of reference pressure is otained by connecting the fluctuating-pressure source to the reference half of the cell by a capillary tube. The movement of the diaphragm is then proportional to the magnitude of the fluctuations. A dynamic calibration of the instrument provided information for making amplitude-response corrections for frequencies from about 5 to 50 cps.

TEST PROCEDURE

Model Preflight Tests

Longitudinal-stability tests.- The results from smooth-air tests of an identical canard model (ref. 2) and a similar tail-last model (ref. 3) were used to determine the longitudinal stability characteristics and their variation with Mach number for the two models of this report. Shown in figure 4 are the static and dynamic longitudinal stability characteristics calculated for the flight conditions of the canard and tail-last models from the stability data of references 2 and 3. Also shown in figure 4 are the stability characteristics of the tailless model of reference 1. The variation of lift-curve slope with Mach number for each model may be found in reference 2.

Vibration tests.- The structural vibration modes, frequencies, and nodal lines of the two models were determined by suspending the models from shock cords attached to forward and rearward sections of the fuselage and mechanically vibrating the model by an electromagnetic shaker mounted at the center of gravity. These results are shown in figure 5 for both models.

Model Tests

The atmospheric and turbulence conditions for forecasting and selecting a suitable test day are described in detail in reference 1. A similar procedure was used for the present test; on the day of a post-cold-front condition with strong offshore winds, an airplane survey was made to determine the suitability of turbulence conditions over the firing range at the Langley Pilotless Aircraft Research Station at Wallops Island, Va., and to determine the intensity and variation with altitude of the turbulence.

The two models, canard and tail-last, were not tested on the same day; however, the same procedure was used for each test. The models were ground-launched at an elevation angle of 25° in order to insure that the tests be conducted at low altitudes (up to 3,000 feet) in the region of existing turbulence conditions. Following separation from their booster-rocket motors, the models experienced decelerating flight for about 8 seconds from $M = 1.0$ to $M = 0.80$. Then sustainer rockets in the models accelerated the models to about $M = 1.1$, after which data were obtained for the second time from $M = 1.0$ to $M = 0.80$. Unfortunately the telemeter did not function for the first decelerating period of the tail-last-model flight and data are presented for only the second decelerating period of the flight. As shown in table I, small differences in weight and moment of inertia existed for the canard model for the conditions of before and after sustainer-rocket burning which resulted in the small differences in dynamic and static stability shown in figure 4.

Turbulence Measurements

Although the models were equipped with the total-pressure-fluctutation instrument, the airplane surveys were still a necessary part of the technique since the final decision for making the tests depended on the airplane pilot's judgment as to the suitability of the turbulence conditions. Also, for the tail-last model the data obtained from the pressure-fluctuation instrument did not appear to be reliable and the survey-airplane data were used as discussed in reference 1 to establish the variation of turbulence intensity with altitude.

On the test days, airplane surveys were made along the firing course at altitudes from 500 to 3,500 feet in 500-foot increments with two test runs, 4 to 5 miles in length, made at each altitude (to-sea and to-land directions). The recorded airspeed-acceleration data at each altitude were evaluated to determine the derived gust velocities U_{d_e} in accordance with the revised gust-load formula. For the tail-last-model test the airplane survey data were used in the following manner to establish the spectra of turbulence encountered by the model at the various altitudes.

In reference 1 some test results are described for an airplane equipped with an airspeed-fluctuation measuring system which established that the shape of the spectrum of horizontal gust velocities could be approximated by the relation

$$\Phi_1(\Omega) = \frac{K}{\Omega^2} \qquad (0.003 < \Omega < 0.5)$$

where K is a constant and is a measure of the turbulence intensity. If this simple relation is also assumed to apply to the spectrum of vertical turbulence, the value of K appropriate to the tail-last-model test conditions was estimated from the relative gust experience U_{d_e} of the survey airplane and the airplane used to obtain the shape of the gust spectrum. For example, the airplane used in establishing the shape of the spectrum indicated a spectrum of $0.052/\Omega^2$ and evaluations from the survey-airplane data indicated that the gust intensities for the tail-last model at the 1,500-foot-altitude condition were roughly 76 percent as severe as those obtained from the airplane flights to determine the spectrum shape. The appropriate value of K for the tail-last model at 1,500 feet would then be $0.052(0.76)^2$ or 0.03 since the spectrum is a function of the gust velocity squared. Shown in table II are the values of K obtained in this manner for the tail-last model.

An examination of the airplane survey data for the canard-model test indicated that the turbulence intensity decreased as the distance from the shore increased, in addition to changing with altitude. Under changing conditions of turbulence of this type the survey-airplane data could not be used to define the level of turbulence experienced by the model for short periods of time or sample lengths. One of the recommendations made in reference 1 for improving the testing technique was to exercise greater selectivity in the choice of test conditions to obtain more homogeneous turbulence. Apparently the survey-airplane pilot was influenced too much by the heavy turbulence near the shore in making the decision to test the model. A fairly satisfactory improvement in the technique has been used in a recent test by telemetering the acceleration data from the survey airplane to a visual recorder on the ground and thus enabling another observer to examine the acceleration trace for suitable test conditions.

Fortunately the spectra of turbulence obtained from the total-pressure-fluctuation instrument for the canard-model test appeared to be a satisfactory indication of the turbulence encountered by the model. Several power spectra of the horizontal component of gust velocity obtained for several portions of the canard-model test are shown in figure 6. The spectra in figure 6 have been corrected for the frequency response of the measuring system which is fairly poor at low frequencies up to 0.05 radian per foot or about 7 cps. The spectra also show

considerable scatter probably due to the short record samples. Curves of the type K/Ω^2, which are shown by the solid lines of figure 6, were fitted to the data to have the same mean-square gust velocity as the data points. The values of K obtained in this manner are shown in table II for the canard model and indicate a large decrease in turbulence intensity for the second decelerating period of the flight after sustainer-motor burning.

RESULTS AND ANALYSIS

Experimental Results

The techniques of generalized harmonic analysis as described in references 1 and 4 are particularly useful in analyzing the gust data from rocket-model tests. Since the models are changing altitude and speed continuously during the tests, the amount of data obtained at fixed conditions is very limited. In general, the data are analyzed for record sections averaging about 2 seconds in length where the change in model forward speed is about 6 percent or less. Then the Mach number indicated for each record section represents an average during this speed change. Since the normal-acceleration data were reduced from the telemeter records at 0.01-second intervals, each record averaged about 200 data points. The direct result of the short sample length is to introduce statistical fluctuations in the data and thus limit the precision of the results.

The results of the basic-data evaluation for the canard and tail-last models for flight in continuous rough air are presented for several of the record sections in the form of time histories (fig. 7) and power-spectral-density functions of normal acceleration (figs. 8 and 9). These results serve the purpose of illustrating the general characteristics of the loads and motion for flight through rough air and are presented as measured; that is, no corrections for differences in turbulence intensity with altitude were made.

The variation of root-mean-square center-of-gravity normal-acceleration increments with Mach number is presented in figure 10 for both models. In order to obtain the variation of the root-mean-square values with Mach number it was necessary to adjust the test results for the difference in turbulence intensity at the various altitudes. Shown in table II are the values of the turbulence intensity appropriate for each record section. These values were used in ratio form to adjust the root-mean-square values of normal acceleration to a gust-velocity spectrum having the equation $\Phi_i(\Omega) = \frac{0.03}{\Omega^2}$.

[redacted]

Analytical Calculations

In order to determine whether the general level and variation with Mach number of the root-mean-square acceleration increment could be predicted by means of power-spectral methods, some theoretical calculations were made for both models. The theoretical basis for determining mean-square loads by means of generalized harmonic analysis is presented in detail in references 1 and 4 and only a brief discussion is presented herein. When the atmospheric turbulence is described by a power-spectral-density function referred to as the input, it is related to the output or aircraft normal-acceleration spectrum through the amplitude squared of the aircraft frequency-response function which is the normal-acceleration response to sinusoidal gust disturbances. The area under the output or normal-acceleration power-spectral-density curve is the mean-square normal acceleration. The spectrum of atmospheric turbulence used in the calculations was

$$\Phi_i(\Omega) = \frac{0.03}{\Omega^2}$$

as previously discussed. The transfer functions were determined as described in reference 1. The procedure assumes that the model in penetrating a sharp-edge gust behaves essentially as a one-degree-of-freedom system (vertical motion only) up to the first peak acceleration. This rather simplified assumption of neglecting pitching motion up to the first peak is probably in greater error for the canard model than for the tail-last model. However, calculations for the canard model using the method of reference 5 showed that for the case of a sharp-edge gust the effect of pitch was inappreciable until after the model had reached its first peak acceleration. The first peak normal-acceleration responses for both the canard and tail-last models were determined from the results of reference 6, along with the experimental values of lift-curve slope obtained from stability tests of references 2 and 3. Beyond the first peak it was assumed that both models responded in the short-period longitudinal motion (both vertical and pitching motion) with the period and damping shown in figure 4. From the model response to a step or sharp-edge gust, the frequency-response function was determined analytically for Mach numbers from 0.80 to 1.0 by the equations given in reference 4. The variation of calculated root-mean-square acceleration obtained for both models is shown in figure 10 for direct comparison with the experimental values.

DISCUSSION

Characteristics of rough-air response.- An examination of several typical time histories of center-of-gravity and nose acceleration for

both the canard and tail-last models (figs. 7(a), 7(b), and 7(c)) indicates that in rough air both models undergo sustained and irregular oscillations composed of frequencies which appear to be anywhere from 4 to about 120 cps. The lowest frequency corresponds to the model short-period longitudinal motion, and the higher frequencies are several of the structural frequencies shown in figure 5. Since the various frequencies present are somewhat mixed on the time-history traces, the power spectra of figures 8 and 9 will provide a better identification of the frequencies.

In figure 7(a) for the tail-last model at $M = 0.80$ the nose and center-of-gravity accelerometers indicate about the same reading for the short-period motion. In figures 7(b) and 7(c) for the canard model the short-period motion is greatly reduced in the nose-acceleration time history compared to the center-of-gravity accelerations. The difference in amplitude of the nose and center-of-gravity readings for the short-period motion is proportional to the angular acceleration in pitch as given by the equation

$$\frac{\Delta n_{nose} - \Delta n_{cg}}{l/g} = \ddot{\theta}$$

where l is the distance in feet between the two accelerometers. For both models the nose accelerometer was located about 3 feet ahead of center of gravity. Therefore, the time histories of figure 7 indicate that the angular acceleration in pitch was smaller for the tail-last model than for the canard model.

The angular acceleration in pitch is directly related to the static longitudinal stability by means of the expression

$$I_Y \ddot{\theta} = qS\bar{c}C_m = qS\bar{c}C_{m_\alpha} \Delta\alpha$$

when the damping in pitch is neglected. The difference in pitching acceleration for the two models is then directly related to the square of the short-period frequency ω_n of figure 4 since

$$\omega_n^2 = \frac{C_{m_\alpha} qS\bar{c}}{I_Y} = \frac{\ddot{\theta}}{\Delta\alpha}$$

For example, from the data of figure 4 at $M = 0.80$ the pitching acceleration $\ddot{\theta}/\Delta\alpha$ for the canard model would be about 2.8 times that of the tail-last model.

The time histories of figures 7(b) and 7(c) correlate with the power spectra of horizontal gust velocity of figure 6 for the canard model in that the large decrease in normal-acceleration amplitude corresponds to a decrease in turbulence intensity for the second portion of the canard-model test.

Power spectra of acceleration increments.- The spectra of figures 8 and 9 are presented primarily for the purpose of identifying the various frequencies illustrated in the time histories of figure 7 and for showing their relative contributions to the total power or mean-square acceleration.

These spectra- with the exception of figures 8(e), 8(f), and 9(e), were computed from the time-history data by using the procedures recommended in reference 7. The data were reduced from the records at 0.01-second intervals with the result that the highest frequency that could be resolved in the spectra was 50 cps. Since the high-frequency components were not faired from the records before computing the spectra, the power densities at frequencies higher than 50 cps are reflected to a small amount in the low frequencies. Forty estimates of power equally spaced over the frequency range of 0 to 50 cps were obtained for each record section shown. As discussed in reference 7, each point on the curves of figures 8(a) to 8(d) and 9(a) to 9(d) represents an estimate of the average power of a frequency band width of 5 cps. The direct effect of this band width is a reduction in sharpness of peak values of these spectra.

Several typical power spectra of normal acceleration for the canard model are shown in figures 8(a) to 8(d) for frequencies from 0 to 50 cps. Spectra of normal acceleration measured 3 feet ahead of the center of gravity are shown in figures 8(a) to 8(d) in addition to the center-of-gravity normal-acceleration spectra. For the center-of-gravity power spectra the greatest concentration of power is at the model short-period frequency of 5 to 7 cps, and there is an indication of a small peak near 35 cps or the wing first bending frequency. However, for the spectra obtained from the nose-accelerometer data, the peak at the short-period frequency is greatly reduced because of angular acceleration in pitch (as previously discussed). The reduced turbulence intensity for the portion of the canard-model flight after sustainer-motor burning (greater distance from the shore) is illustrated by the reduced ordinate scale of figures 8(a) and 8(b) compared with figures 8(c) and 8(d). In order to obtain spectra which include the higher frequencies, several record sections were analyzed by means of a magnetic-tape harmonic analyzer and are shown in figures 8(e) and 8(f) for the same record sections as figures 7(b), 7(c), 8(b), and 8(c). The high-frequency peak is near 120 cps and an examination of figure 5 shows that this frequency is near a body bending mode for the canard model. At a frequency of 120 cps, the spectra of figures 8(e) and 8(f) have been corrected for the frequency response of the accelerometer, since at this frequency the amplitude indicated is only about 0.40 of the actual amplitude. The difference in the height of the peak at the short-period frequency of figures 8(b) and 8(c) compared

with figures 8(e) and 8(f) from the magnetic-tape analyzer is probably due to some difference in the filter width for the tape analysis.

The power spectra for the tail-last model shown in figure 9 are similar to those for the canard model. A comparison of the peaks at the short-period frequency for the nose and center-of-gravity accelerations indicates that the angular acceleration in pitch was less than that indicated for the canard model. The spectrum of figure 9(e) obtained from the magnetic-tape analyzer indicates that a high-frequency peak near 100 cps or a body vibration mode is also present for the tail-last model. At a frequency of 100 cps the amplitude of the center-of-gravity accelerometer readings is about 0.76 of the actual amplitude.

Variation of acceleration with Mach number.- The measured root-mean-square accelerations are shown in figure 10 as a function of Mach number for both the canard and tail-last models. The data of figure 10 have been corrected to the same turbulence intensity by means of table II which lists the values of K in the equation of the turbulence spectrum $\Phi_i(\Omega) = \frac{K}{\Omega^2}$ for the various record sections. The values of root-mean-square normal acceleration of figure 10 correspond to an input spectrum of atmospheric turbulence having a value of $K = 0.03$. However, the data of figure 10 still include the different weight and moment of inertia for each model listed in table I. Since the values of σ of figure 10 are proportional to the integrals of the power spectra of figures 8 and 9 from 0 to 50 cps, they include a small amount of the power at 100 to 120 cps which was reflected at the lower frequencies.

With the large amount of scatter shown in figure 10 it is difficult to establish any definite variation of root-mean-square acceleration with Mach number or to make comparisons of the canard and tail-last models other than the general level of the load intensity. With the short sample lengths of data it is possible for statistical fluctuations to cause discrepancies or scatter of the order of ± 20 percent. If the variation of σ with Mach number depends primarily on the variation of damping in pitch with Mach number, then it can be seen from the damping data of figure 4 that the difference in the variation of σ with Mach number for the canard and tail-last rocket models is a small-order effect and is masked in the scatter of the data.

Curves of calculated root-mean-square normal acceleration are shown in figure 10 for comparison with the experimental values. The calculated values were obtained from the simplified transfer functions previously discussed along with an input spectrum $0.03/\Omega^2$. The calculated curves include only the short-period frequency since no attempt was made to include structural frequencies in the transfer functions. In general there is fair agreement in the general level of the experimental and calculated values.

In order to summarize the results from the three rocket-powered models that have been tested in rough air, the experimental root-mean-square normal accelerations for the tailless (ref. 1), tail-last, and canard models are shown in figure 11 as a function of Mach number. The data of figure 11 have been corrected to the same turbulence intensity $0.03/\Omega^2$ and represent a wing loading of 22.7 lb/sq ft for all three models. As can be seen in figure 4, there is a large variation of time to damp to one-half amplitude with Mach number for the tailless model and this variation is reflected in the variation of σ with Mach number in figure 11 with the exception of one point at $M = 0.81$. In a qualitative sense the experimental values of σ for each model reflect the variation of time to damp to one-half amplitude for each model. The large amplification of load intensity due to the decreased pitch damping of the tailless model from $M = 0.8$ to 1.0 is not seen in the data for the canard and tail-last models.

CONCLUDING REMARKS

Results from rocket-model flight tests in continuous rough air at Mach numbers from 0.8 to 1.0 at low altitudes have been presented for a canard and a tail-last configuration having the same wing and tail surfaces. The technique used in testing rocket models in rough air appears to lack the precision necessary for investigating small-order effects. However, considerable improvement in the technique was realized by using an airspeed-fluctuation instrument in the canard model to measure the turbulence intensity experienced by the model. This instrument, which measures fluctuations in total pressure, is still in the development stage but appears to be a better indication of the turbulence experienced by the models than the survey-airplane data. The survey airplane is still a necessary part of the technique since it is necessary to select carefully the test days for homogeneous turbulence required for the relatively short model flights. As mentioned in a previous investigation, the precision of the results could be improved by obtaining longer samples at each test condition.

The experimental data for the canard and tail-last models showed that the short-period frequency was dominant in the center-of-gravity normal-acceleration response. This was also shown by a sharp peak in the power-spectral-density functions of normal acceleration at the short-period frequency for both models. As illustrated by differences in center-of-gravity and nose normal acceleration, the canard model experienced larger values of angular acceleration in pitch due primarily to greater static stability. The variation of root-mean-square normal acceleration with Mach number did not show any significant difference between the canard and tail-last models probably because of lack of precision in test results. However, when the variation of the root-mean-square normal acceleration with Mach number was compared for the previously tested tailless model and the canard and

tail-last models, the effect of the improved damping in pitch of the canard and tail-last models could be seen in a qualitative sense in that the curves for all three models reflected the variation of time to damp to one-half amplitude with Mach number.

Langley Aeronautical Laboratory,
National Advisory Committee for Aeronautics,
Langley Field, Va., November 30, 1954.

REFERENCES

1. Vitale, A. James, Press, H., and Shufflebarger, C. C.: An Investigation of the Use of Rocket-Powered Models for Gust-Load Studies With an Application to a Tailless Swept-Wing Model at Transonic Speeds. NACA TN 3161, 1954.

2. Vitale, A. James, and McFall, John C., Jr.: Longitudinal Stability Characteristics at Transonic Speeds of a Canard Configuration Having a 45° Sweptback Wing of Aspect Ratio 6.0 and NACA 65A009 Airfoil Section. NACA RM L54I01, 1954.

3. McFall, John C., Jr.: Longitudinal Stability Characteristics at Transonic Speeds of a Rocket-Propelled Model on an Airplane Configuration Having a 45° Swept Wing of Aspect Ratio 6.0. NACA RM L53G22a, 1954.

4. Press, Harry, and Mazelsky, Bernard: A Study of the Application of Power-Spectral Methods of Generalized Harmonic Analysis to Gust Loads on Airplanes. NACA Rep. 1172, 1954. (Supersedes NACA TN 2853.)

5. Donely, Philip, Pierce, Harold B., and Pepoon, Philip W.: Measurements and Analysis of the Motion of a Canard Airplane Model in Gusts. NACA TN 758, 1940.

6. Mazelsky, Bernard: Charts of Airplane Acceleration Ratio for Gusts of Arbitrary Shape. NACA TN 2036, 1950.

7. Tukey, John W.: The Sampling Theory of Power Spectrum Estimates. Symposium on Applications of Autocorrelation Analysis to Physical Problems (Woods Hole, Mass.), June 13-14, 1949, pp 47-67. (Sponsored by ONR, Dept. Navy.)

TABLE I.- MODEL MASS CHARACTERISTICS

Canard Model

	Before sustainer-motor burning	After sustainer-motor burning
W, lb	99.6	89.6
Center-of-gravity position, positive rearward, percent $\bar{c}$	-125	-131.5
I_Y, slug-ft^2	10.48	10.14

Tail-Last Model

	After sustainer-motor burning
W, lb	86.9
Center-of-gravity position percent $\bar{c}$	21.2
I_Y, slug-ft^2	8.39

TABLE II.- VALUES OF K FOR THE CANARD AND THE TAIL-LAST MODELS

M	h, ft	K for equation $\Phi_i(\Omega) = \frac{K}{\Omega^2}$
Canard Model		
0.940	600	0.0235
.890	900	.0571
.840	1,060	.0284
1.015	1,120	.0034
.940	1,000	.0041
.895	810	.0137
.855	550	.0059
Tail-Last Model		
1.040	2,650	0.0370
.971	2,655	.0370
.920	2,410	.0340
.884	2,050	.0278
.850	1,600	.0288
.818	1,035	.0294
.800	400	.0332

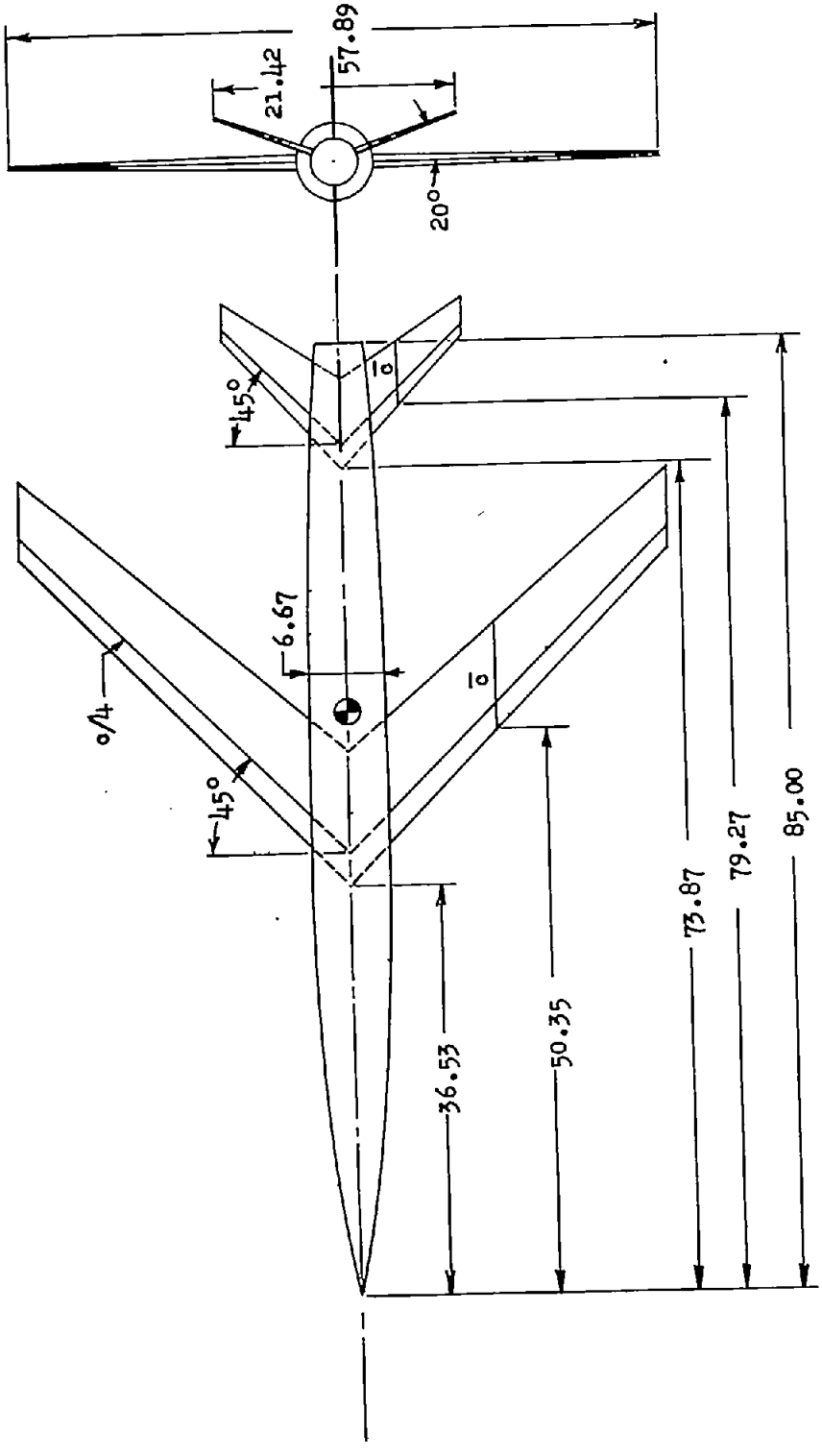

WING
Airfoil NACA 65A009
A 6.00
S(total) 3.88 sq ft
c̄ 9.85 in.
c(root) 12.06 in.
c (tip) 7.24 in.
Dihedral 0 deg

HORIZONTAL FINS
Airfoil NACA 65A006
A 4.00
S(total) .90 sq ft
c̄ 6.05 in.
c(root) 8.15 in.
c (tip) 3.26 in.
Dihedral −20 deg
Incidence 0 deg

Figure 1.- Tail-last configuration (all dimensions in inches).

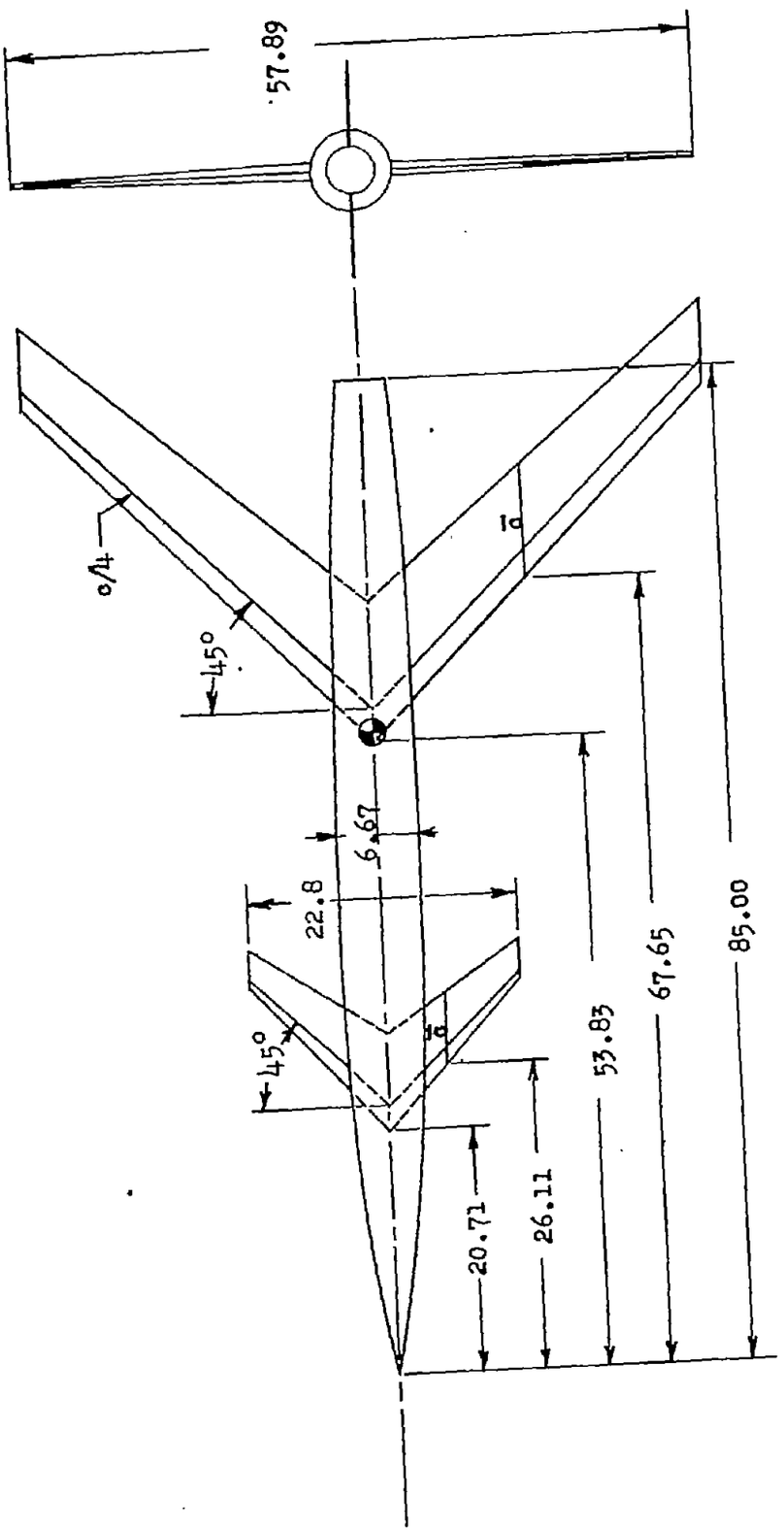

WING
Airfoil NACA 65A009
A 6.00
S(total) 3.88 sq ft
$\bar{c}$ 9.85 in.
c(root) 12.06 in.
c (tip) 7.24 in.
Dihedral 0 deg

CANARD FINS
Airfoil NACA 65A006
A 4.00
S(total) .90 sq ft
$\bar{c}$ 6.05 in.
c(root) 8.15 in.
c (tip) 3.26 in.
Dihedral 0 deg
Incidence 0 deg

Figure 2.- Canard configuration (all dimensions in inches).

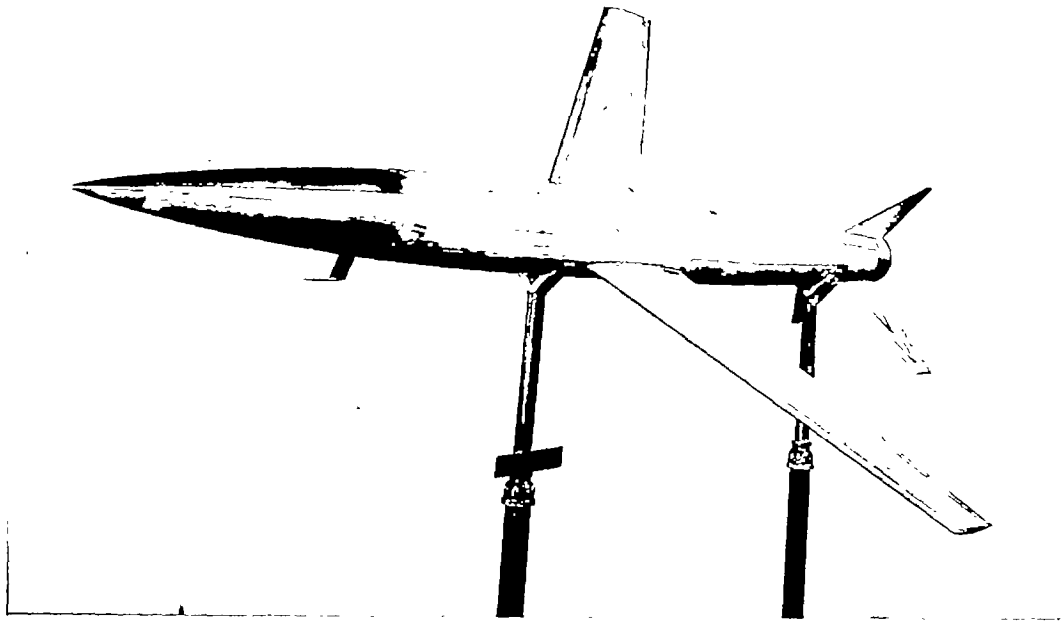

(a) Tail-last model. L-79438.1

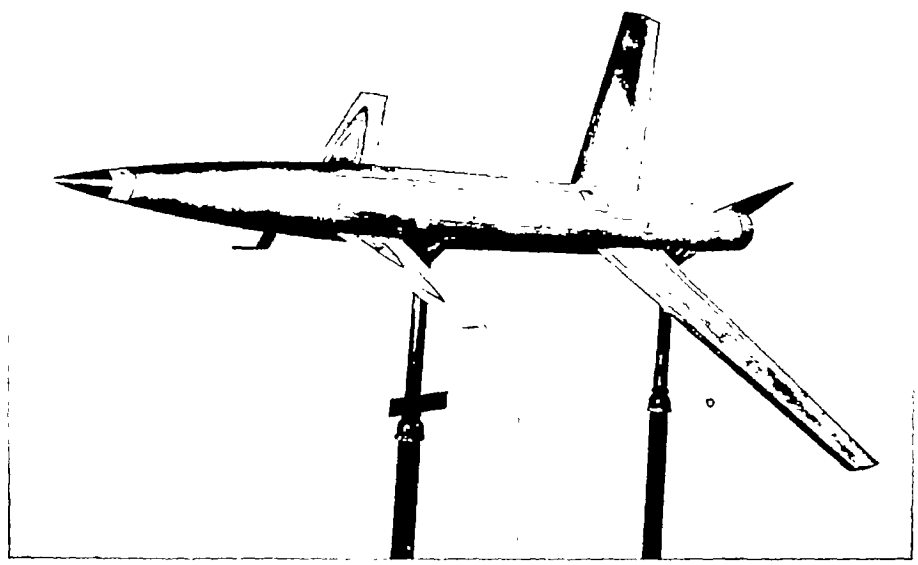

(b) Canard model. L-79440.1

Figure 3.- Photographs of models.

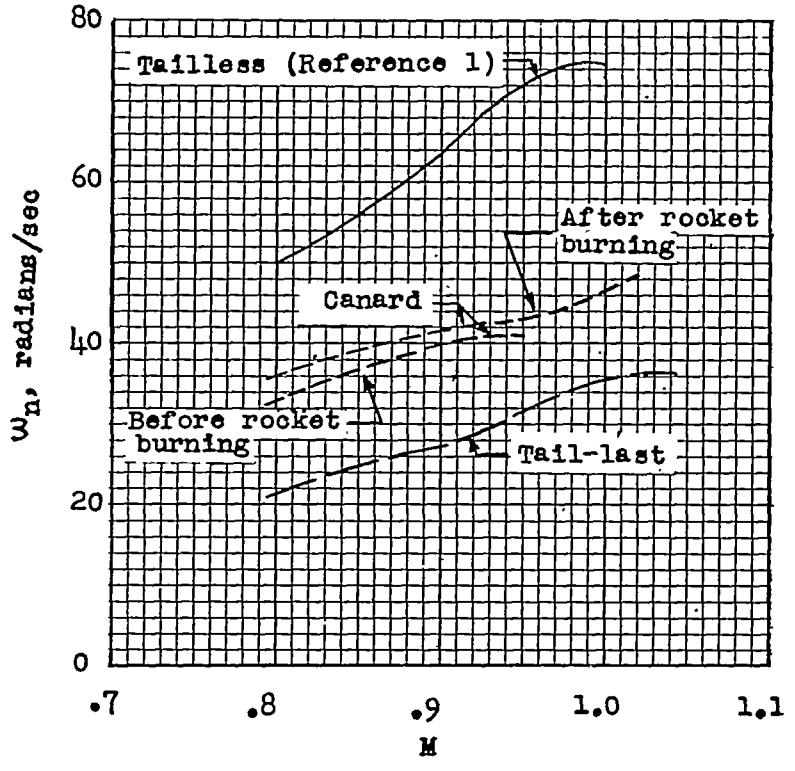

(a) Variation of undamped natural frequency with Mach number.

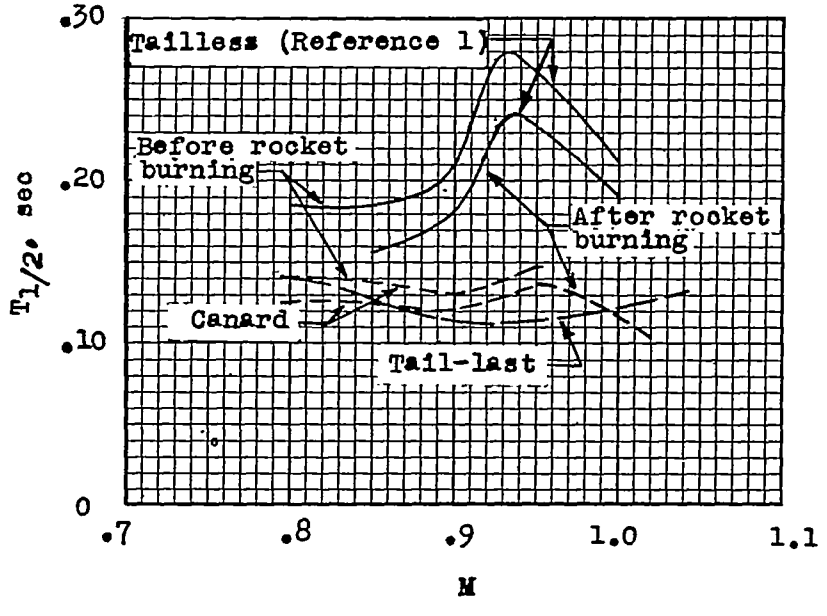

(b) Variation of time to damp to one-half amplitude with Mach number.

Figure 4.- Longitudinal stability characteristics of models.

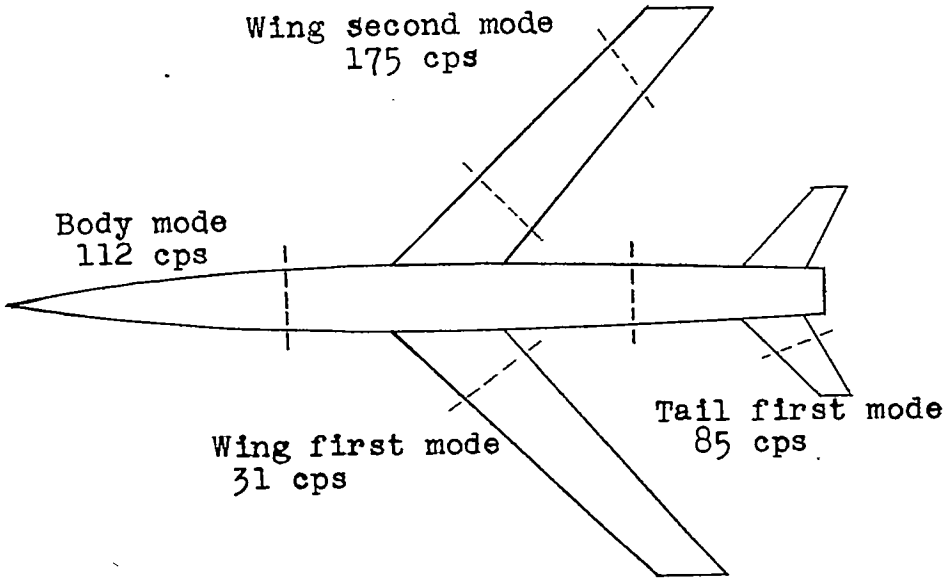

(a) Tail-last model.

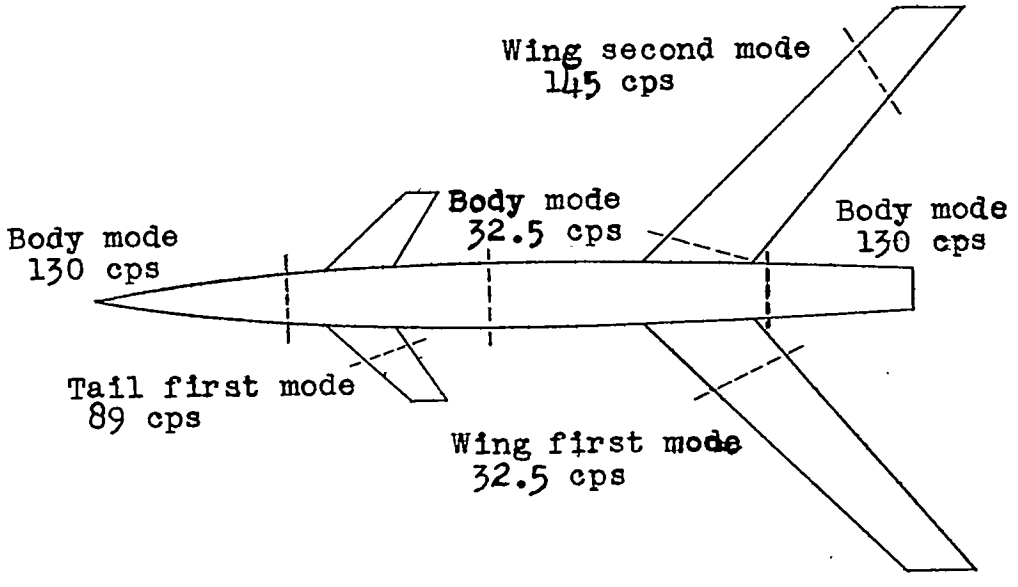

(b) Canard model.

Figure 5.- Model vibration frequencies. Node lines for the various modes are indicated by dashed lines.

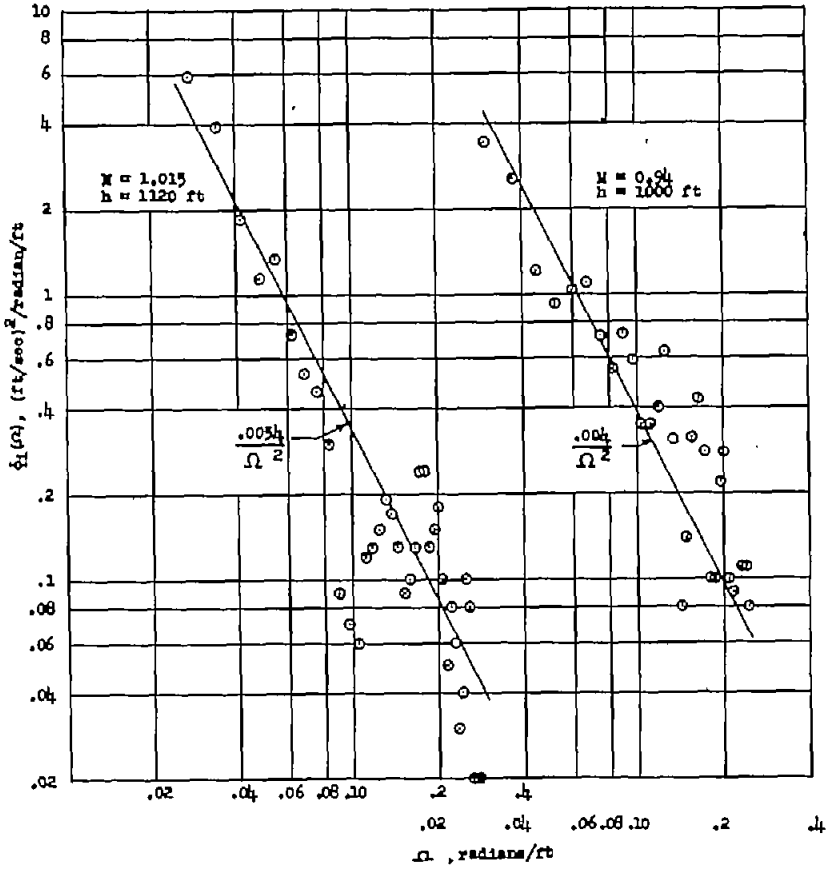

(a) Low-level turbulence for portion of model flight after sustainer-motor burning.

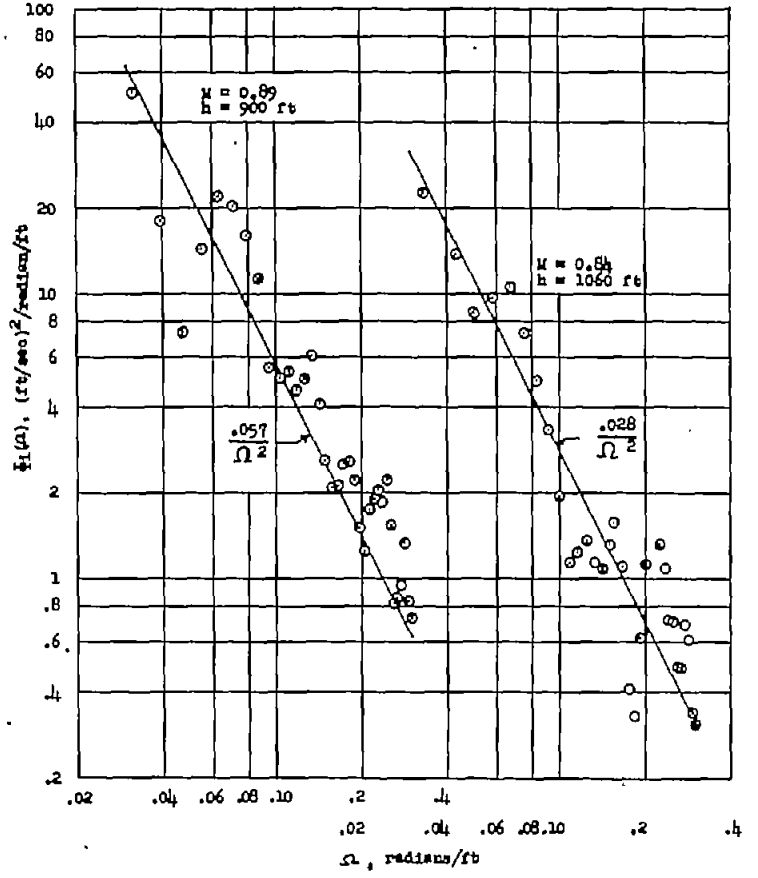

(b) High-level turbulence for portion of model flight before sustainer-motor burning.

Figure 6.- Power-spectral-density functions of atmospheric turbulence for the canard-model test obtained from airspeed-fluctuation data.

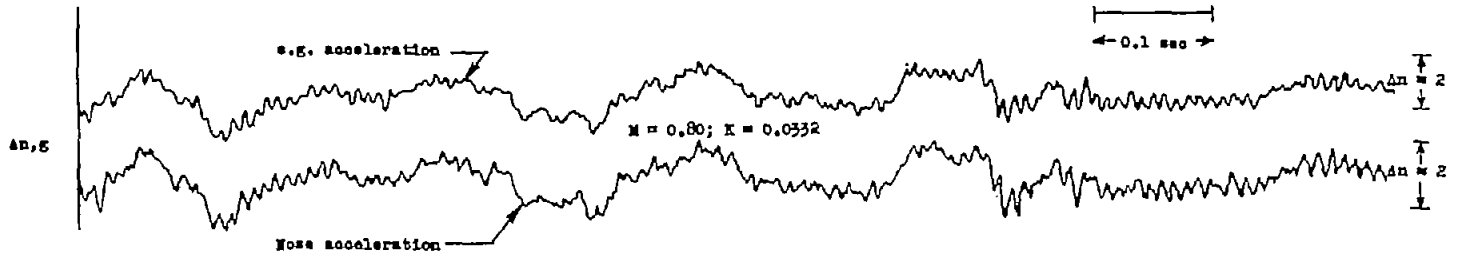

(a) Tail-last model.

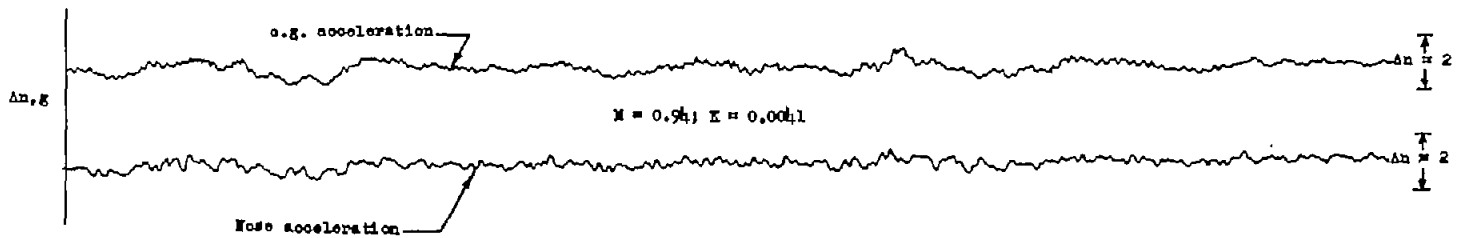

(b) Canard-model flight in low-level turbulence after sustainer-motor burning.

(c) Canard-model flight in high-level turbulence before sustainer-motor burning.

Figure 7.- Time histories of normal acceleration.

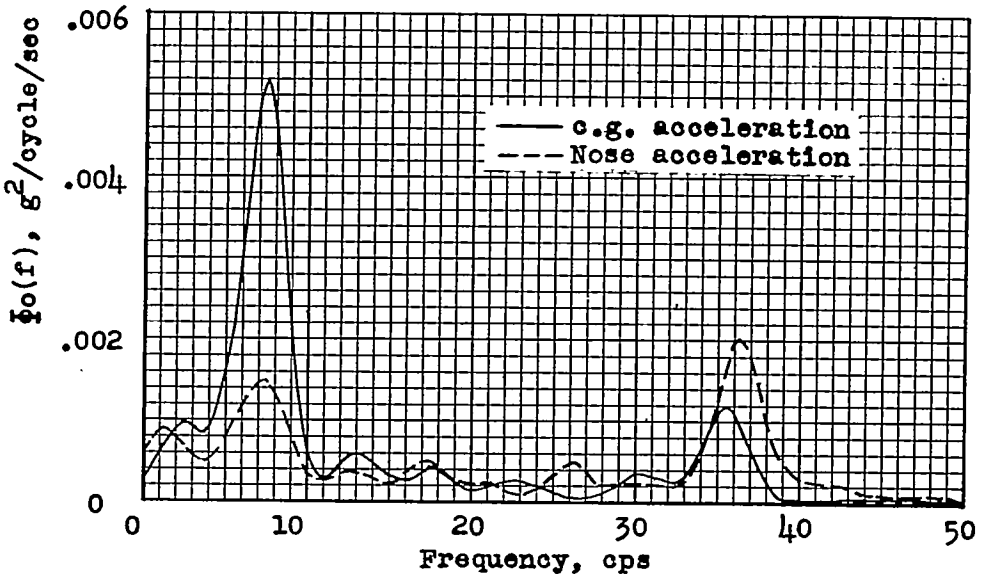

(a) M = 1.015; K = 0.0034 (after sustainer burning).

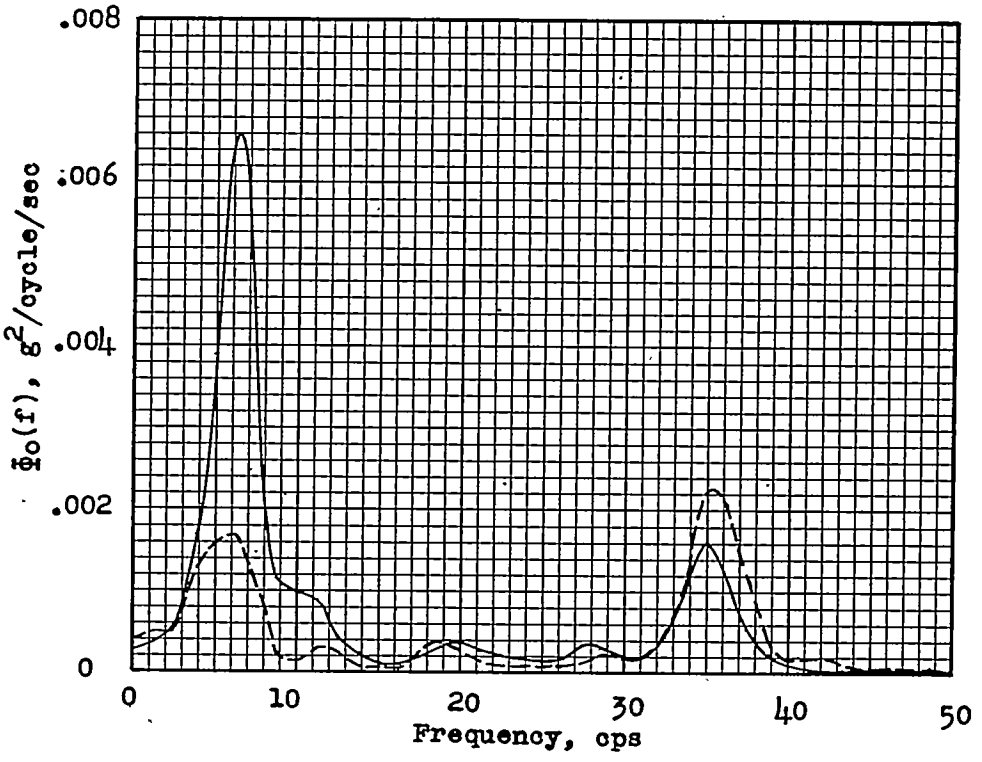

(b) M = 0.94; K = 0.0041 (after sustainer burning).

Figure 8.- Power-spectral-density functions of normal-acceleration data for the canard model.

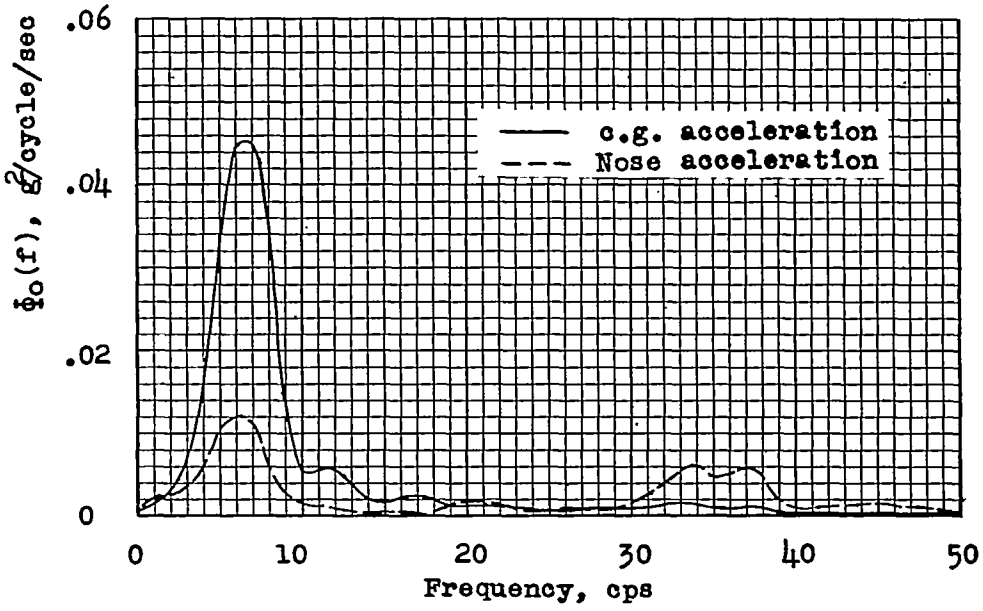

(c) M = 0.89; K = 0.0571 (before sustainer burning).

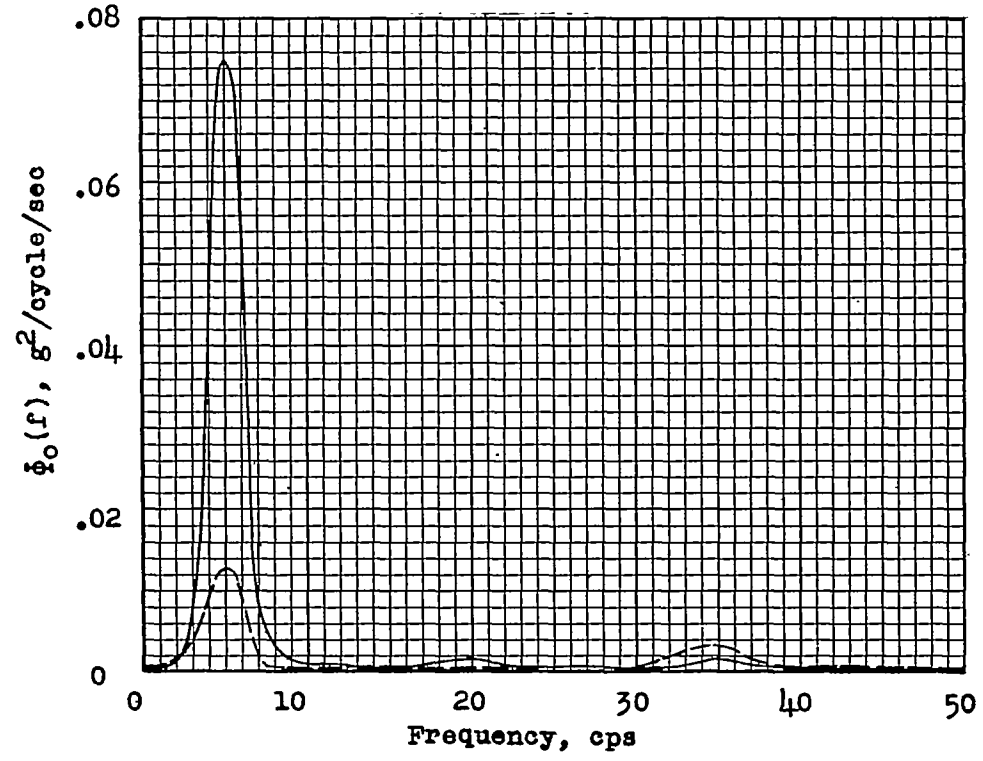

(d) M = 0.84; K = 0.0284 (before sustainer burning).

Figure 8.- Continued.

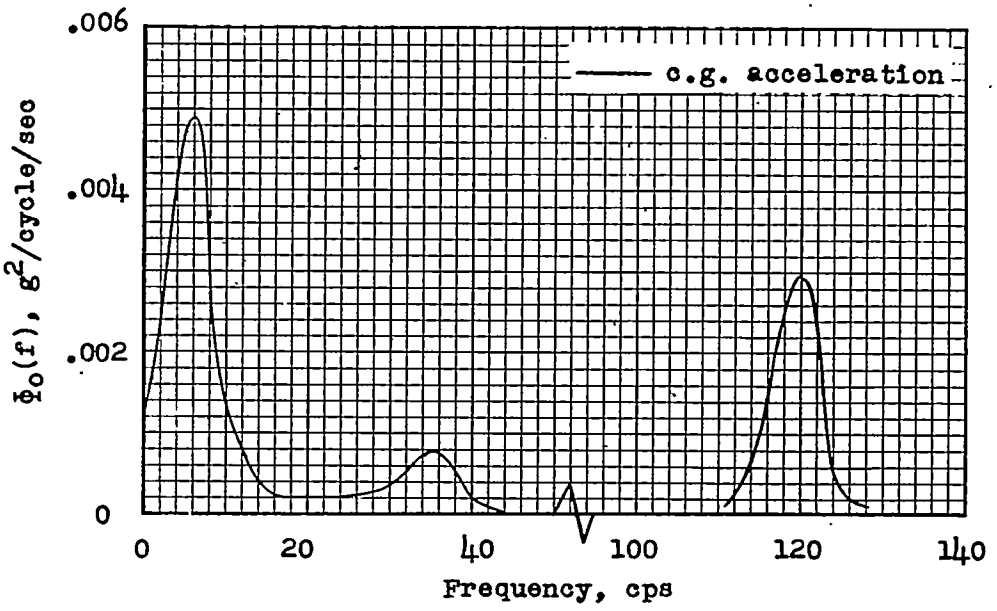

(e) Power spectrum from magnetic-tape analyzer. M = 0.94; K = 0.0041.

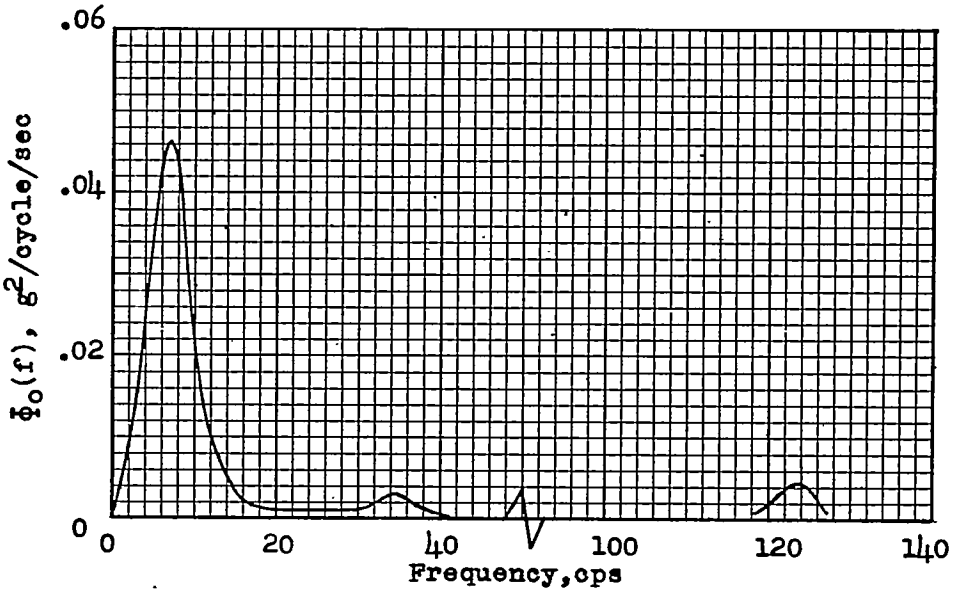

(f) Power spectrum from magnetic-tape analyzer. M = 0.89; K = 0.0571.

Figure 8.- Concluded.

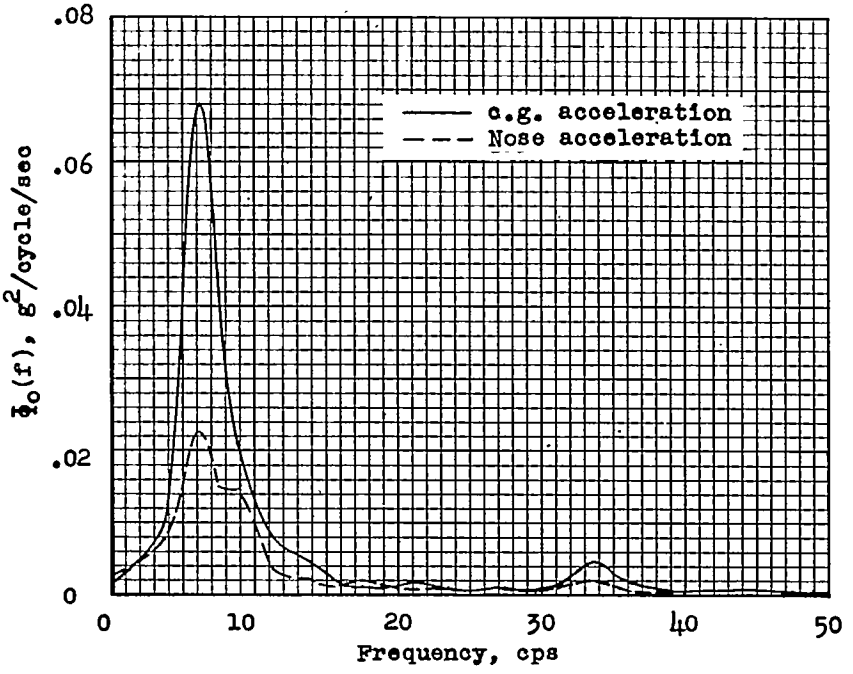

(a) M = 1.04; K = 0.0370.

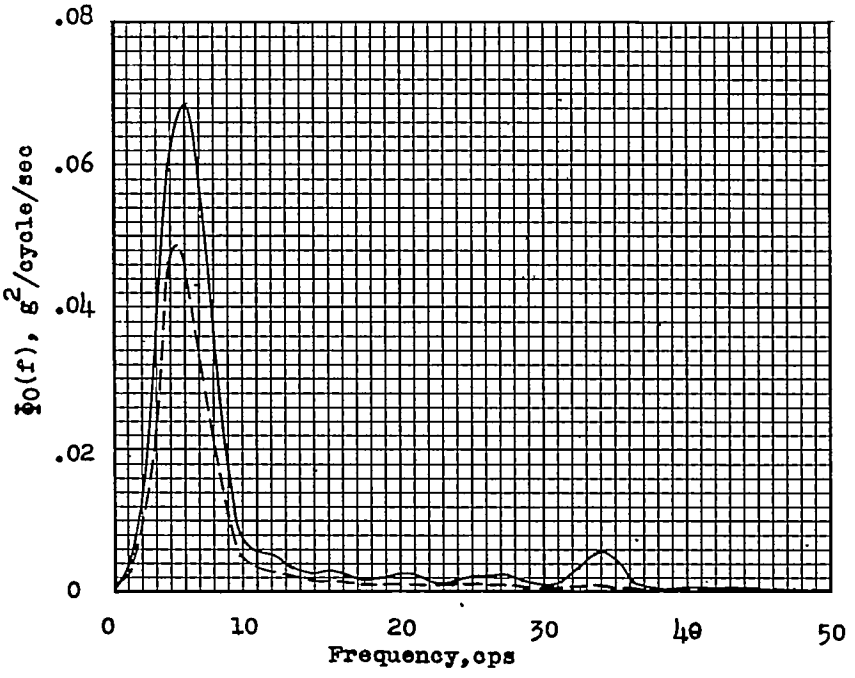

(b) M = 0.92; K = 0.0340.

Figure 9.- Power-spectral-density functions of normal-acceleration data for the tail-last model.

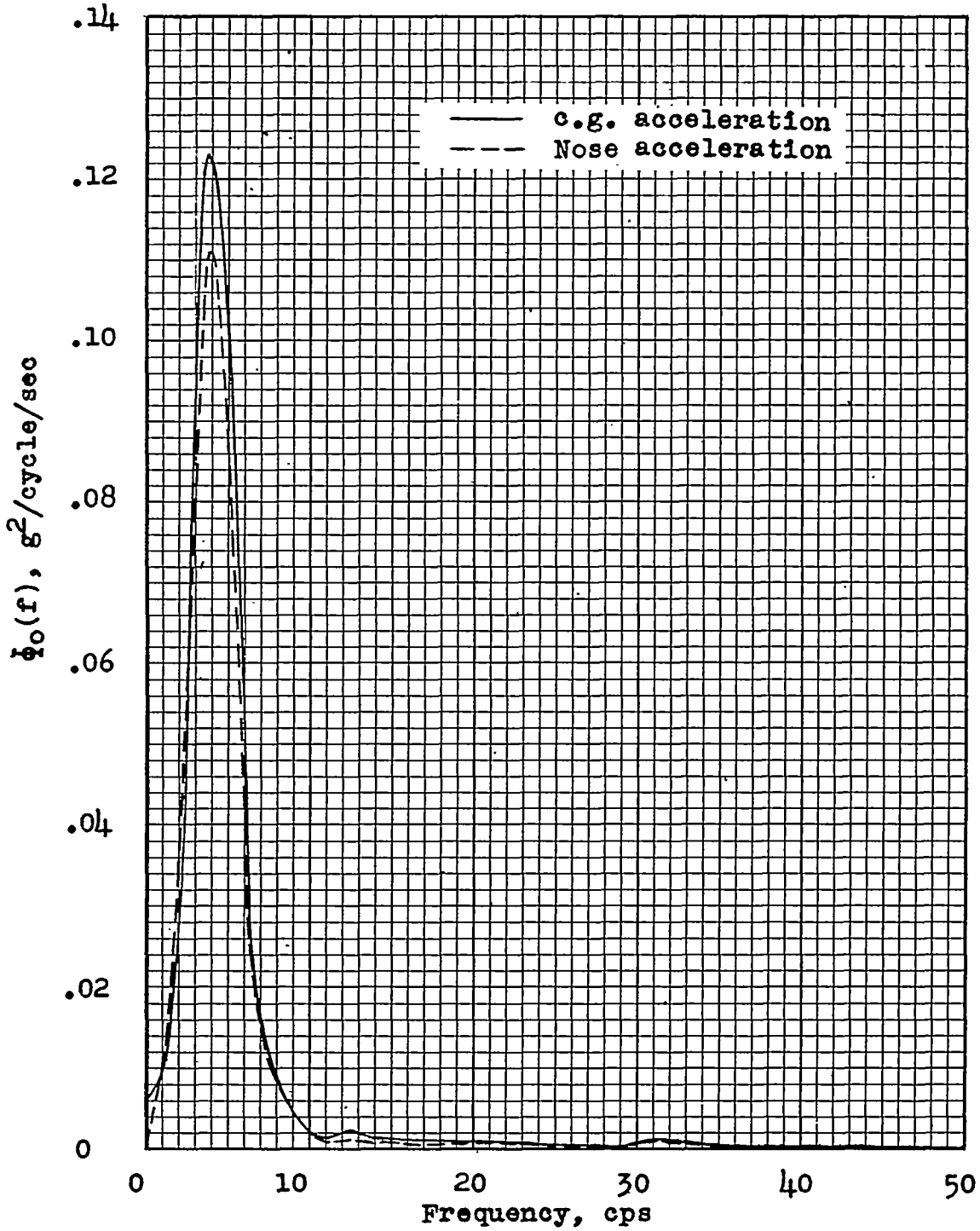

(c) M = 0.85; K = 0.0288.

Figure 9.- Continued.

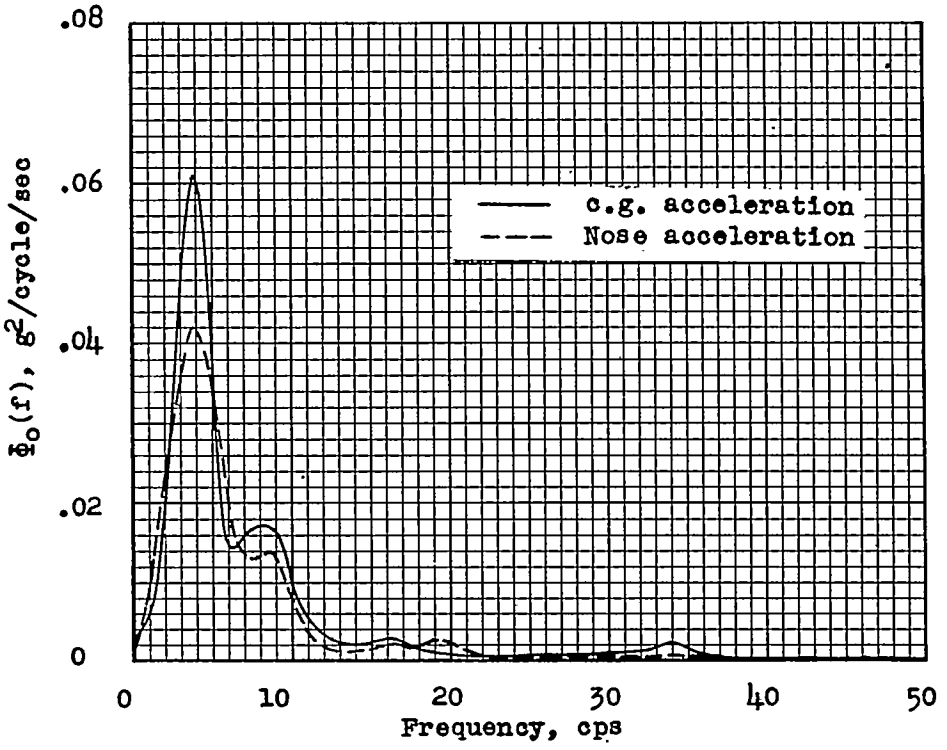

(d) M = 0.80; K = 0.0332.

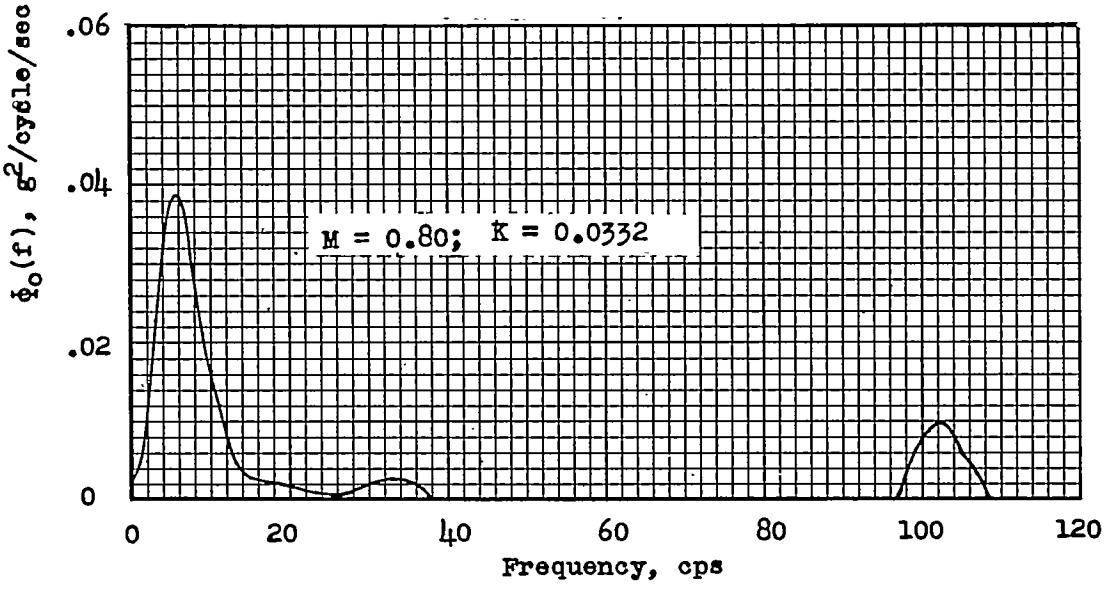

(e) Power spectrum from magnetic-tape analyzer showing high-frequency peak.

Figure 9.- Concluded.

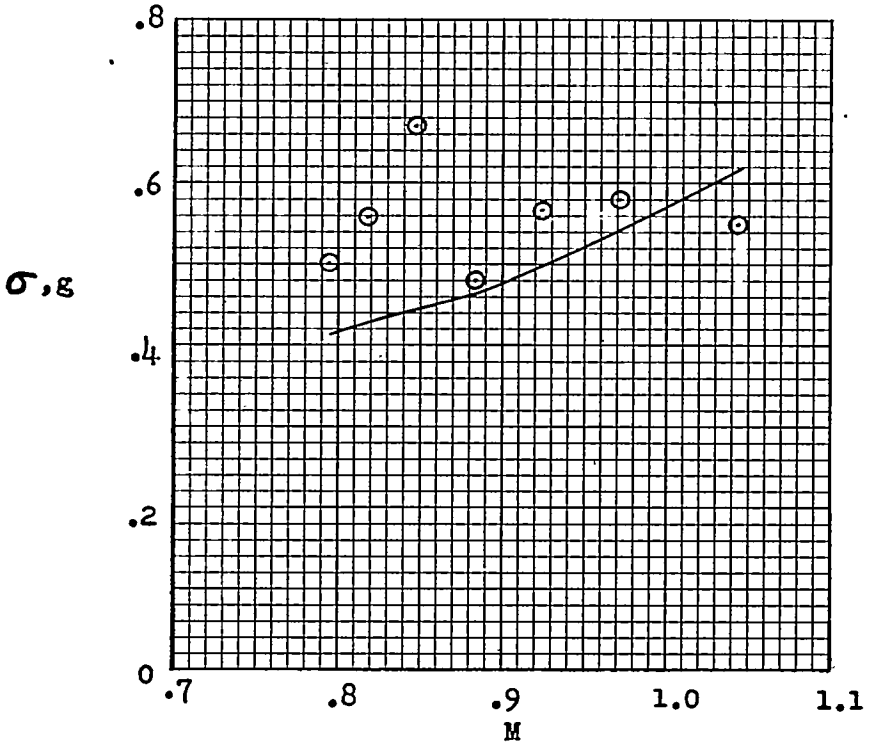

(a) Tail-last model.

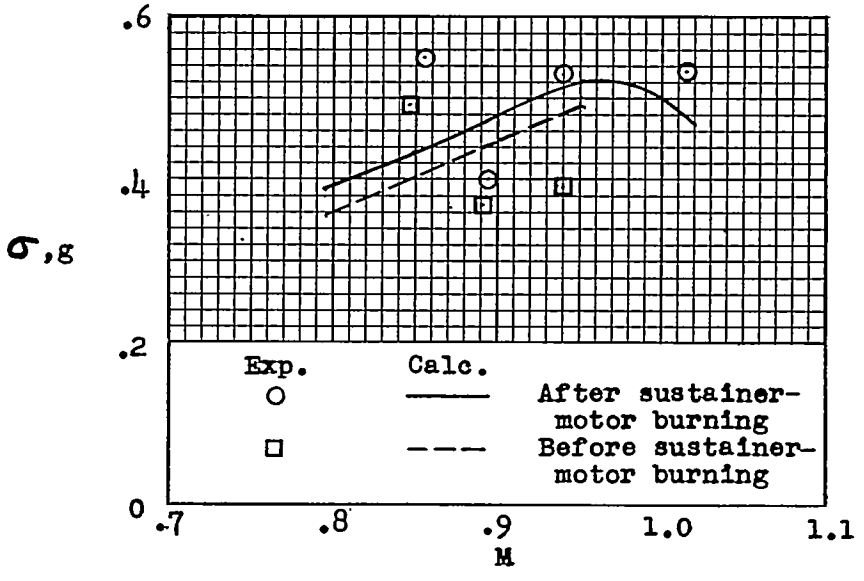

(b) Canard model.

Figure 10.- Variation of experimental and calculated root-mean-square normal acceleration with Mach number.

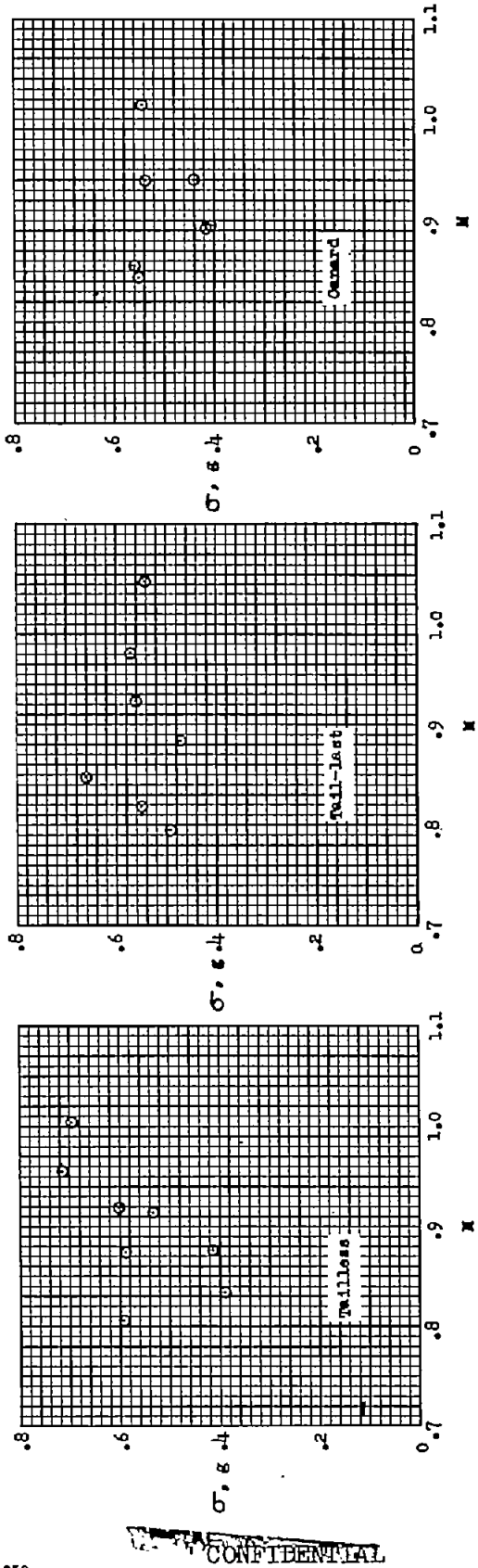

Figure 11.- Variation of root-mean-square normal acceleration with Mach number of tailless (ref. 1), tail-last, and canard models for a wing loading of 22.7 lb/sq ft.

NACA-Langley - 3-1-55 - 350